


Article

# Robotic-Arm-Based Force Control in Neurosurgical Practice

Ibai Inziarte-Hidalgo <sup>1,2</sup> , Irantzu Uriarte <sup>1</sup>, Unai Fernandez-Gamiz <sup>1</sup> , Gorka Sorrosal <sup>3</sup>  and Ekaitz Zulueta <sup>1,\*</sup><sup>1</sup> University of the Basque Country (UPV-EHU), 48940 Leioa, Spain<sup>2</sup> Research & Development Department, Montajes Mantenimiento Y Automatismos Electricos Navarra S.L., 01010 Vitoria-Gasteiz, Spain<sup>3</sup> Ikerlan Technology Research Centre, Basque Research and Technology Alliance (BRTA), 20500 Arrasate-Mondragon, Spain

\* Correspondence: ekaitz.zulueta@ehu.eus; Tel.: +34-945014160

**Abstract:** This research proposes an optimal robotic arm speed shape in neurological surgery to minimise a cost functional that uses an adaptive scheme to determine the brain tissue force. Until now, there have been no studies or theories on the shape of the robotic arm speed in such a context. The authors have applied a robotic arm with optimal speed control in neurological surgery. The results of this research are as follows: In this article, the authors propose a control scheme that minimises a cost functional which depends on the position error, trajectory speed and brain tissue force. This work allowed us to achieve an optimal speed shape or trajectory to reduce brain retraction damage during surgery. The authors have reached two main conclusions. The first is that optimal control techniques are very well suited for robotic control of neurological surgery. The second conclusion is that several studies on functional cost parameters are needed to achieve the best trajectory speed of the robotic arm. These studies could attempt to optimise the functional cost parameters and provide a mechanical characterisation of brain tissue based on real data.

**Keywords:** neurosurgical robotics; optimal control; optimal speed shape**MSC:** 49-11

**Citation:** Inziarte-Hidalgo, I.; Uriarte, I.; Fernandez-Gamiz, U.; Sorrosal, G.; Zulueta, E. Robotic-Arm-Based Force Control in Neurosurgical Practice. *Mathematics* **2023**, *11*, 828. <https://doi.org/10.3390/math11040828>

Academic Editor: António Lopes

Received: 3 January 2023

Revised: 25 January 2023

Accepted: 31 January 2023

Published: 6 February 2023



**Copyright:** © 2023 by the authors. Licensee MDPI, Basel, Switzerland. This article is an open access article distributed under the terms and conditions of the Creative Commons Attribution (CC BY) license (<https://creativecommons.org/licenses/by/4.0/>).

## 1. Introduction

According to the authors of [1], an estimated 22.6 million patients suffer neurological injuries each year, of which 13.8 million require surgery. According to the American Association of Neurological Surgeons (AANS), approximately 50,000 neurosurgeries lasting more than half an hour are performed annually in the United States alone. Furthermore, research presented in [2] indicated that brain tissue begins to experience stress/tension a quarter of an hour after the onset of retraction. In general, clinically significant postoperative deficits occur in 3–9% of cases, although there is considerable variation depending on the difficulty of the applied procedure [3,4]. An incidence of approximately 10% of retraction-related complications has been recorded in skull base surgery. These complications include parenchymal haematomas, aphasia, hemiparesis and numbness. In addition, a study of posterior circulation aneurysm surgery reported that 4% of patients suffered retraction-induced brain injury [5]. In the case of pineal region tumours, two out of twelve patients had permanent visual defects which the authors attributed to occipital lobe retraction [6].

A study by Laha et al. [7] indicated that if the mean arterial pressure exceeds the brain's retraction pressure by less than 70 mmHg, the brain will be damaged. When this difference is greater than 200 mmHg, the brain recovers completely. Other authors [8] have proposed that regional cerebral blood flow (rCBF) should be greater than 10–13 mL 100 gm<sup>-1</sup> min<sup>-1</sup>; otherwise, there is an imminent danger of ischaemic brain damage.

Minimally invasive surgery (MIS) is an alternative technique to conventional surgery that allows surgical procedures to be performed without the need for large incisions [9]; one

common tool used in this area is the steerable catheter, which has recently become the object of considerable research interest [10]. The most notable benefits for patients associated with this technique include fewer surgical complications and, depending on the case, a shorter operating time, reduced postoperative pain, shorter hospital stay, faster recovery times, less stress on the immune system and lower hospital costs [11,12]. One of the major areas within MIS is minimally invasive robotic surgery (MIRS), which incorporates the use of robotic systems to enhance the surgeon's skills. The development of these surgical robots is motivated by the desire to both systematise and improve the efficiency of the procedure by providing information regarding actions performed in the operating room and to reduce human physical limitations during surgery and other interventional procedures while nonetheless retaining human control [2].

Sometimes, during intracranial procedures, to reach the damaged area to be treated, the neurosurgeon must perform a manoeuvre called brain retraction. This manoeuvre consists of retracting part of the brain to access deeper parts of the brain, as shown in Figure 1. Similar techniques are applied in other settings, e.g., hernia repair [13].

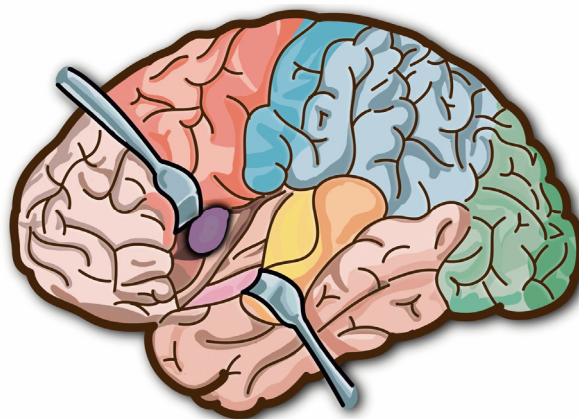


**Figure 1.** Brain retraction.

However, despite its being an essential practice for adequate tissue exposure, retraction can result in brain contusions and/or infarctions [9,11,12,14]. According to the authors of [2], the pressure exerted on the brain surface during retraction causes a variety of forms of damage depending on the magnitude of the retraction, the time of execution and the site of application. This pressure is transferred to the adjacent brain tissue, causing subsequent deformation and partial or total closure of blood vessels, thereby disrupting the oxygen supply to brain cells. The severity of brain damage depends on factors such as retractor pressure distribution, geometry, physical properties and type of brain tissue, vascular pressure and the duration of retraction [15].

However, these are not the only factors to be considered during retraction; gravity, blood and cerebrospinal fluid loss, as well as certain anaesthetic agents, can cause a non-rigid deformation of up to 20 mm in the shape of the brain during surgery [16–18], which, coupled with variation in brain stiffness [16–23], makes it even more difficult to obtain adequate and safe retraction.

Nowadays, surgical robots provide fundamental support to surgeons during a large range of operations, principally in MIS [24]. Hoeklemann et al. [25] highlighted three fundamental types of surgical robotic system capabilities: (1) teleoperated (master–slave) systems, in which the robotic system is controlled from an operating console via a human–machine interface and the robot executes the motion commands it receives (e.g., the da Vinci robot); (2) image-guided systems, where the robot executes a pre-established surgical plan in the pre-operative phase based on intraoperative geometric information acquired by a navigation or tracking system; and (3) active guidance, where the surgeon manually guides the robot to move surgical instruments to the desired position [16].

Among surgical robots, the da Vinci robot is the current reference, although a great deal of other surgical robotic equipment exists, depending on the area to be treated. In the neurological field, the Robotised Stereotactic Assistant System (ROSA) is one of the most popular robotic systems on the market today [26].

However, ROSA cannot perform all of the procedures that may be required during a neurological intervention.

To protect the brain during prolonged surgery, a monitoring and/or control system is necessary to ensure that certain safety requirements are met. Although there have been numerous studies on the use of robotics in neurosurgery (for example, [27,28]), these have not addressed brain retraction, and the vast majority of advances made in this field are related to the development of the retractors themselves [29,30] or the development of mechanical models and simulators aimed at training surgeons [22,31,32]. No studies or technological developments have been described for the robotic control of brain retraction.

The main objective of this paper is to introduce a proposed control law to improve robotic neurosurgery, i.e., by setting the brain extensor speed as a function of position error and the force experience by the brain tissue. This paper also presents a theoretical justification of the proposed technique.

## 2. Problem Settlement and Control Proposal

Generally, in neurosurgery practice, the brain retractor keeps the brain tissue sufficiently retracted to be able to access the area where the lesion (tumour, stroke, etc.) is located. When these retractors open brain tissue, they can induce ischaemic processes. Such processes can generate clinically significant postoperative deficits and even death. Therefore, there are two main objectives: to retract enough brain tissue and to minimise ischaemic damage.

The first objective is to achieve access to a physical location, as defined by the physician; this point is called  $x_{desired}$ . Brain retractors retract the brain tissue to the  $x$  position. The second objective is to keep force  $F$  applied by the brain retractors as low as possible.

The dynamics of the robotic arm are not relevant, as the speeds of its trajectories are lower than the bandwidth of the robotic arm. The robotic arm traces linear trajectories in which the displacement is very small. Additionally, the robotic arm has its own control unit that is capable of following the speed set point with a negligible margin of error. Finally, the brain tissue forces are not big enough to generate relevant following errors in terms of positioning, so the speed set point can be assumed to be the real brain tissue speed. The dynamics of the robotic arm may be defined by Equation (1).

$$\frac{dx}{dt} = u \quad (1)$$

Brain tissue generates a reaction force when the retractors are opened by the robotic arm. The authors have modelled this force using the hyperelastic response from the Ogden model [33] (see Figure 2). Other approaches can be used to model the brain tissue deformation force, e.g., [34], although they are too complex for control applications. Usually, the system models applied in control applications must be as simple as possible in order to give results in control sample time.

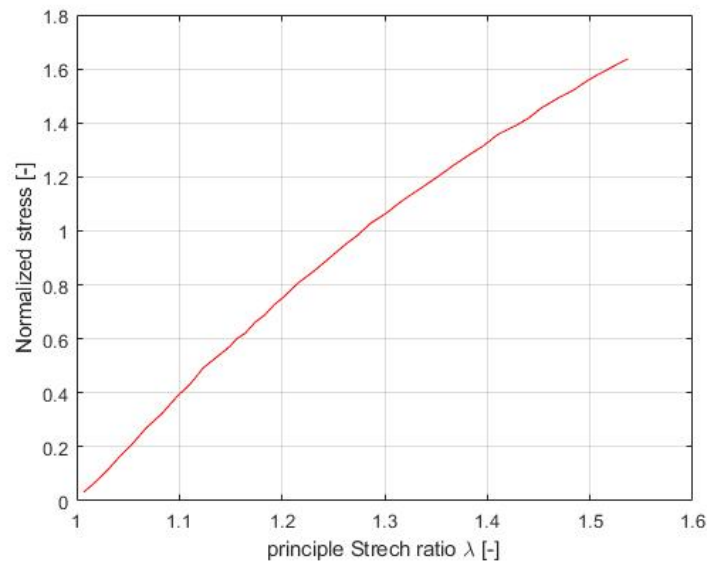


Figure 2. Ogden model for brain tissue.

$$\alpha = \frac{x + L_{initial}}{L_{initial}} \tag{2}$$

The force applied by the brain retractor depends on  $\lambda$  and time. These dependencies are described in [33,35]. The force depends on the brain retractor contact surface (approximately 1 cm<sup>2</sup>) and the maximum pressure. The maximum pressure, i.e.,  $Pressure_{max}$ , can be found in [36]. In our study, this parameter was set to 500 Pa. The relationship between the force applied by the brain retractors and the normalised force are given in Equations (3) and (4).

$$F = F_{max} \cdot F_{Normalized}(\alpha, t) \tag{3}$$

$$F_{max} = A \cdot Pressure_{max} \tag{4}$$

### 3. Control Proposal

To prevent ischaemia and other damage during brain retraction, the authors propose the application of a variational calculus-based control law. One of the most difficult things in optimal control laws is to set a correct cost functional; therefore, the authors first performed the following analysis.

#### 3.1. Cost Functional Proposal

The authors propose that the position error should be included in this cost functional. Another variable that must be in the cost functional is the brain force. This force is defined in Equations (2)–(4). Finally, the brain retraction speed must be in this functional state. Therefore, the authors could incorporate these all conditions in the following cost functional proposal. Here,  $f_{cost}$  is a function that was chosen for this section and  $\lambda_v$  is the speed ponderation coefficient.

$$J = \int_0^{T_{max}} f_{cost}(x_d - x, F(x)) \cdot dt + \lambda_v \int_0^{T_{max}} \dot{x}^2 \cdot dt \tag{5}$$

The authors imposed further boundary conditions. The first condition ensured that the final position of the robotic brain retractor was the desired position. The second condition was that the final speed had to be equal to zero. Finally, the third condition was that the initial position of the robotic brain retractor was equal to zero.

$$x(T_{max}) = x_{desired} \tag{6}$$

$$\dot{x}(T_{max}) = 0 \tag{7}$$

$$x(0) = 0 \tag{8}$$

We then applied the Euler–Lagrange equation and the transversal conditions in order to fulfil Equation (6). Attention should be drawn to the fact that  $T_{max}$  is not a constant value. This aspect imposes a transversal condition.

$$J = \int_0^{T_{max}} (f_{cost}(x_{desired} - x, F(x)) + \lambda_v \dot{x}^2) \cdot dt \tag{9}$$

$$J = \int_0^{T_{max}} G(x, \dot{x}) \cdot dt \tag{10}$$

To optimise Equation (5), the Euler–Lagrange equation must be applied. With the aim of fulfilling Equation (6), a transversal condition has been proposed; see Equation (12).

$$\frac{\partial G(x, \dot{x})}{\partial x} - \frac{d}{dt} \left( \frac{\partial G(x, \dot{x})}{\partial \dot{x}} \right) = 0 \tag{11}$$

$$G(x, \dot{x}) - \dot{x} \cdot \frac{\partial G(x, \dot{x})}{\partial \dot{x}} \Big|_{t=T_{max}} = 0 \tag{12}$$

Equations (11) and (12) can be defined as follows:

$$\frac{\partial f_{cost}}{\partial x} - 2\lambda_v \ddot{x} = 0 \tag{13}$$

$$\frac{\partial f_{cost}}{\partial x} - \dot{x} \cdot 2\lambda_v \dot{x} \Big|_{t=T_{max}} = 0 \tag{14}$$

Equation (13) was used to define the control trajectory dynamics. Equation (14) defines the transversal condition (see Equation (6)). Equation (15) shows that the optimal trajectory fulfils the following differential equation.

$$\ddot{x} = \frac{1}{2\lambda_v} \frac{\partial f_{cost}}{\partial x} \tag{15}$$

The cost functional must fulfil other mathematical conditions. The  $G$  cost function must be zero when  $x$  is in the initial position, because, in that case, the robot arm does not cause any brain damage. In addition, the  $G$  function must be zero when  $x$  is at  $x_{desired}$ , because the robotics arms must open up to this final position, despite the brain force not being zero.

$$f_{cost}(x_{desired} - x, F(x))|_{x=x_{desired}} = 0 \tag{16}$$

$$f_{cost}(x_{desired} - x, F(x))|_{x=0} = 0 \tag{17}$$

Since the speed is zero in the final position, Equation (14) imposes that  $\frac{\partial f_{cost}}{\partial x}$  is equal to zero when the robot arm reaches the final position at the final time.

$$\frac{\partial f_{cost}}{\partial x} \Big|_{x=x_{desired}} = 0 \tag{18}$$

The authors have proposed the following  $f_{cost}$  function to fulfil Equations (16)–(18).

In order to justify the cost function, we considered the following two main objectives: to retract enough brain tissue, i.e., the brain retractors reach their desired position, and minimising ischaemic damage, i.e., applying as little force as possible with the brain retractors.

Taking these objectives into account, the authors have considered that the cost functional must include the position error on the one hand and the brain force and brain retraction speed on the other as part of the control law. The function defined this way complies with the applied transversal conditions and Euler-Lagrange equation.

$$f_{cost} = \lambda_F(x_d - x)^2 \cdot F^2(x) + \lambda_{error}(x_d - x)^2 \tag{19}$$

### 3.2. Control Law Proposal

The authors propose control law Equation (20). This equation can be obtained from Equations (15) and (19).

$$\ddot{x} = \frac{(x_d - x)}{2\lambda_v} \left[ -2\lambda_F \cdot F^2(x) - 2\lambda_{error} + 2\lambda_F(x_d - x) \cdot F(x) \cdot \frac{\partial F(x)}{\partial x} \right] \tag{20}$$

Equation (20) is a second-order differential equation, where the second derivative of position depends on the  $x$  position only. Therefore, this dynamic imposes a speed with  $x$  as an independent variable. Equation (21) describes the optimal speed shape. This equation was obtained by multiplying the result of Equation (20) by the speed, after the integration both sides.

$$\frac{v^2}{2} - \frac{v_0^2}{2} = \int_0^x \frac{(x_d - x)}{2\lambda_v} \left[ -2\lambda_F \cdot F^2(x) - 2\lambda_{error} + 2\lambda_F(x_d - x) \cdot F(x) \cdot \frac{\partial F(x)}{\partial x} \right] \cdot dx \tag{21}$$

Equation (20) defines a speed function of  $x$ , defined as  $D(x)$ . We once again note that the final speed must be zero, and therefore, the initial speed is defined by  $G(x_d)$ . This condition (see Equation (22)) implies that the force is known and constant. Nevertheless, a more detailed analysis (see Equation (23)) shows that the robot depends only on the position and force; the control system can measure these two variables.

$$D(x) = \int_0^x \frac{(x_d - x)}{2\lambda_v} \left[ -2\lambda_F \cdot F^2(x) - 2\lambda_{error} + 2\lambda_F(x_d - x) \cdot F(x) \cdot \frac{\partial F(x)}{\partial x} \right] \cdot dx$$

$$D(x) = \frac{\lambda_F(x_d - x)^2 F^2(x) + \lambda_{error}(x_d - x)^2}{2\lambda_v}$$

$$\frac{v^2}{2} - \frac{v_0^2}{2} = D(x) \rightarrow \frac{v_0^2}{2} = D(x_d) \tag{22}$$

Therefore, the optimal speed may be determined as follows:

$$v(x) = \sqrt{\frac{\lambda_F(x_d - x)^2 F^2(x) + \lambda_{error}(x_d - x)^2}{2\lambda_v}} \tag{23}$$

It is easy to see that  $D(x_d)$  is zero. The authors conclude that the speed of the robotic arm is a position- and force-dependent function.

## 4. System Setup and Results

The authors propose the following control scheme (see Figure 3). The robotic arm speed is a proposed function (see Equation (23)) that depends on its position and force. These dependencies allow the control to be more adaptive to the patient’s brain tissue force. This control law has three arbitrary lambda coefficients which model the general behaviour of the robotic arm speed. These three coefficients must be correctly defined to achieve the correct speed shape. The relevant parameters and variables are shown in Tables 1 and 2.

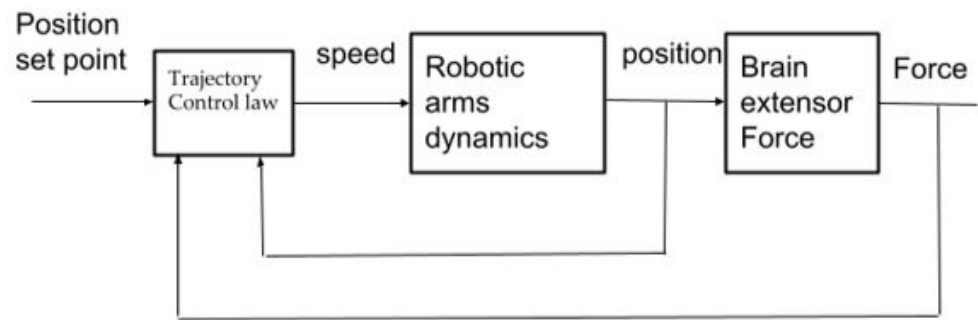


**Figure 3.** The proposed method as a control structure. This proposed technique is a variational/calculus-based one.

The authors developed a control setup to verify the proposed control scheme (see Figure 4). This brain retractor has force measurement units. As the skull imparts a large rigidity to brain tissue, the next main objective was to develop a brain tissue model with water flow tubes to achieve more realistic mechanical behaviour.

The control scheme proposal has three inputs: position set point, position and force (see Figure 3). This control scheme only has one output: speed. This speed is the speed set point for the robotic arm. We considered that the speed set point and the real speed should be equal, because the robotic arm control loops were able to follow the trajectory (the robotic arm had a very large bandwidth) very well.

We incorporated two sensors: a triaxial accelerometer sensor and a set of strain gauges. The strain gauges measure the force applied to the brain tissue through mechanical deformation. We positioned this sensor in the area that suffers from the greatest deformation. The triaxial accelerometer served to measure the weight in order to compensate for gravity. This sensor was position on the rear of the retractor.

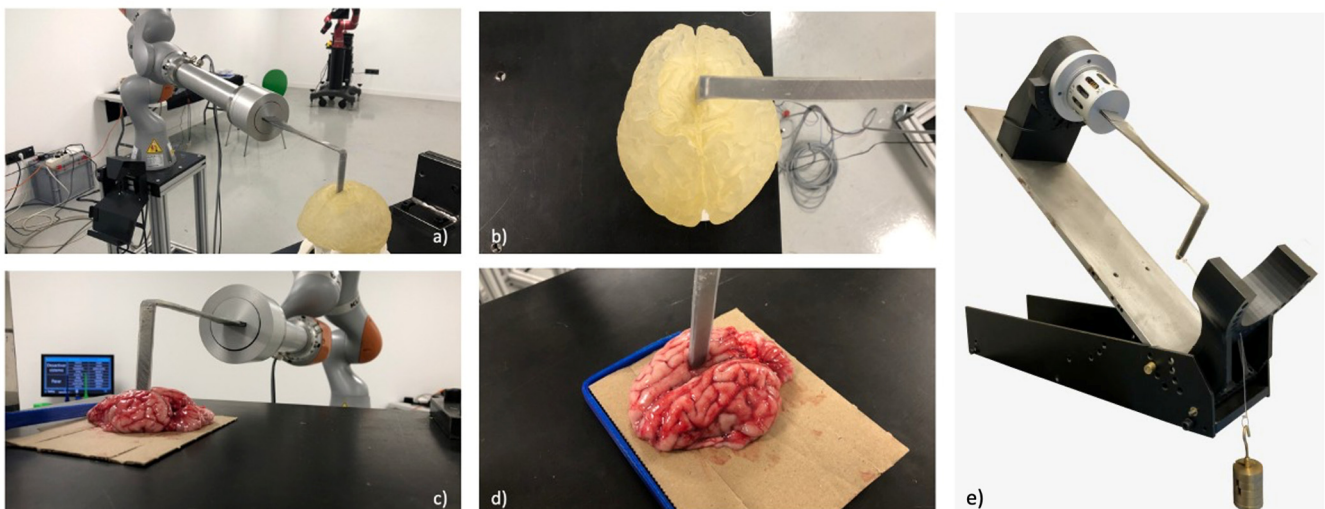


**Figure 4.** (a,b) robotised brain retraction in a 3D printed brain. (c,d) robotised brain retraction in a pig's brain. (e) Sensorised brain retractor calibration.

Table 1 presents the constants of the control system. We applied IS units; the most important variables of the control proposal are shown in Table 2. In Table 1, there are three important parameters:  $\lambda_{error}$ ,  $\lambda_F$  and  $\lambda_v$ . Brain surgeons use these parameters to achieve correct trajectories. These parameters define the maximum speed, the maximum acceleration and the maximum brain tissue force, respectively, as well as the trajectory execution time ( $T_{max}$ ; see Equation (9)). Our application defines the remaining parameters. The force model parameters are given in [28].

**Table 1.** System and control parameters.

Parameter Name	Definition	Value with Units
$F_{max}$	Maximum force amplitude	0.05 N
$A$	Brain retractor contact surface area	1 cm <sup>2</sup>
$Pressure_{max}$	Maximum pressure in brain tissue	500 Pa
$\lambda_{error}$	square position setpoint error ponderation coefficient	10 <sup>-4</sup> m <sup>-2</sup>
$\lambda_F$	square force term ponderation coefficient	1 N <sup>-2</sup>
$\lambda_v$	square speed term ponderation coefficient	10 <sup>-3</sup> s <sup>2</sup> m <sup>-2</sup>
$x_d$	Displacement set point	0.02 m
$L_{initial}$	displaced brain tissue length	m

System parameters.

**Table 2.** System and control variables.

Parameter Name	Definition	Units
$\alpha$	brain tissue stretch	[-]
$x$	brain tissue displacement	m
$v$	Robot arm speed or brain tissue speed	m.s <sup>-1</sup>
$F$	Applied force by brain retractors	N
$F_{Normalized}(x, t)$	Normalised force	[-]

System variables.

### 5. Results

Figures 5–8 present the dynamic behaviour of our proposed method. In Figure 5, we show the robotic arm speed. There is a positive speed at position zero; movement starts, and the speed increases until a maximum value is reached. This maximum depends on the lambda parameters. In the current study, we set the lambda parameters in such a way as to achieve the minimum values for the cost functional. The speed at the final position is zero. It is important to note that the robotic arm speed is the output variable of the control scheme. This speed is the robotic arm speed set point input. We considered that the real speed and robotic arm speed were equal.

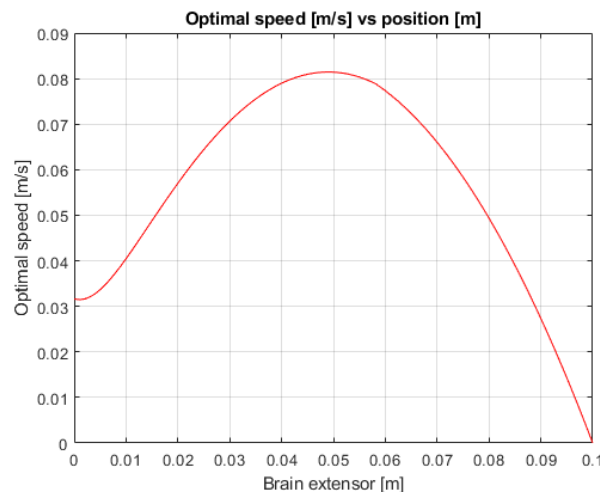


**Figure 5.** Robotic arm speed vs. position.



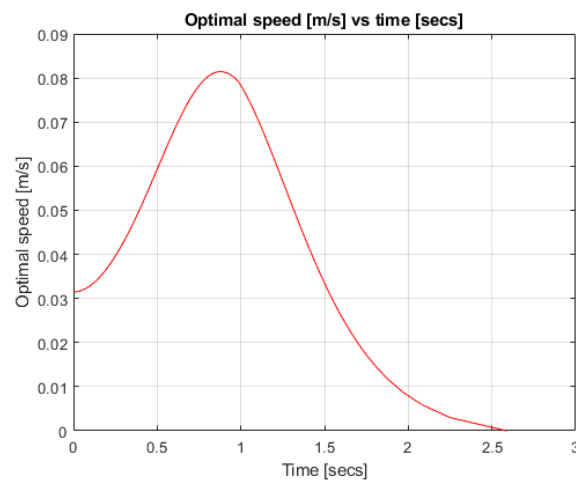


Figure 6. Robotic arm speed over time.

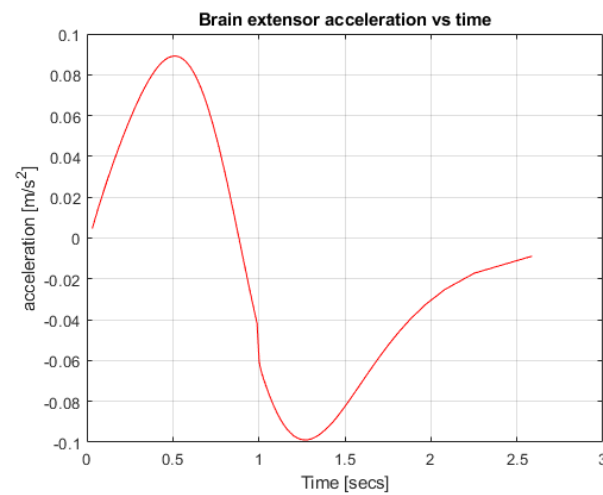


Figure 7. Robotic arm acceleration over time.

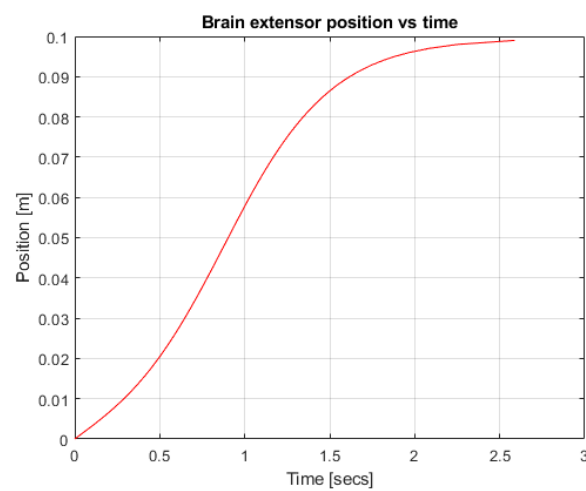


Figure 8. Robotic arm position over time.

Figure 6 illustrates the robotic arm speed over time. Thus, the trajectory execution time depends on the speed shape and on the associated lambda parameters.

Figure 7 shows acceleration over time, i.e., how the lambda parameter values change the maximum acceleration values. In this case, the minimum values (the negative ones) are

as important as the maximum values. These data allowed the authors to set appropriate lambda parameter coefficients.

Figure 8 shows the robotic arm position over time. This shape of this curve illustrates the general behaviour of our control system.

The data presented in Figures 5–8 allowed the authors to select the optimal lambda parameters.

## 6. Conclusions

We have modelled an optimal control problem, where the most important contribution can be seen from the problem settlement and the proposed cost function. It has been shown that the proposed optimal speed shape makes a very important contribution in terms of achieving the best speed shape. The functional proposed in this work (see Equations (9) and (20)) and its optimal speed shape (see Equation (23)) comprise a very good control law that allows the control speed to be adapted to the brain tissue force. The authors suggest that more adaptive approaches could be proposed as deep reinforcement learning techniques; such techniques could then be applied to our research to improve and adapt the control law. Unfortunately, there is no good solution, as such techniques are real data-dependent. The proposed method (see Equation (23)) has been shown to be a very good way to initialise intelligent optimisation techniques.

In the future we will arbitrarily set the lambda coefficient values. These parameters must be set to achieve good acceleration and trajectory execution times. We suggest that these parameters should be set following maximum acceleration and trajectory execution time criteria. Three parameters ( $\lambda_{error}$ ,  $\lambda_F$  and  $\lambda_v$ ) may therefore be set in an arbitrary way. We concluded that these parameters influence two main questions in the trajectory: acceleration and execution time. In the authors' opinion, the biggest limitation of the proposed control scheme is the application of arbitrary values to  $\lambda_{error}$ ,  $\lambda_F$  and  $\lambda_v$ . With this in mind, we expect that expertise on the part of surgeons can solve this problem. These parameters can be automatically optimised with an optimisation algorithm like the Nelder-Mead Simplex Method or Particle Swarm Optimisation. These algorithms are very well suited to such trade off optimisation problems. The next step in our research is to identify the best values for maximum speed, maximum acceleration and maximum brain tissue force.

**Author Contributions:** Conceptualisation, E.Z. and I.I.-H.; methodology, I.I.-H. and E.Z.; software, E.Z. and I.I.-H.; validation, I.U. and U.F.-G.; formal analysis, G.S. and E.Z.; investigation, I.I.-H. and I.U.; resources, U.F.-G. and E.Z.; writing—original draft preparation, I.I.-H. and E.Z.; writing—review and editing, U.F.-G. and I.U. All authors have read and agreed to the published version of the manuscript.

**Funding:** The authors were supported by the government of the Basque Country through the research grant ELKARTEK KK-2021/00014 BASQNET (Estudio de nuevas técnicas de inteligencia artificial basadas en Deep Learning dirigidas a la optimización de procesos industriales). This study has also been conducted partially under the framework of the project MODELO (Grants for R&D projects—2021 and supported by the European Regional Development Funds), ADA project (Grants for R&D projects—2022 and supported by the European Regional Development Funds).

**Data Availability Statement:** Data is available upon reasonable request to the corresponding author.

**Acknowledgments:** The authors acknowledge all support given by Mikel Millan Fernandez de Landa due to its technical support. The authors would also like to thank Karnele Gomez for her contribution. In addition, the authors would also like to thank David Gallego for his technical support and contributions. The authors wish to thank Aldakin Group for its material support. Finally, the authors thank the University of the Basque Country for its laboratory resource collaboration.

**Conflicts of Interest:** The authors declare no conflict of interest.

## References

1. Dewan, M.C.; Rattani, A.; Fiegggen, G.; Arraez, M.A.; Servadei, F.; Boop, F.A.; Johnson, W.D.; Warf, B.C.; Park, K.B. Global Neurosurgery: The Current Capacity and Deficit in the Provision of Essential Neurosurgical Care. Executive Summary of the Global Neurosurgery Initiative at the Program in Global Surgery and Social Change. *J. Neurosurg.* **2019**, *130*, 1055–1064. [[CrossRef](#)]
2. Bennett, M.H.; Albin, M.S.; Bunegin, L.; Dujovny, M.; Hellstrom, H.; Jannetta, P.J. Evoked Potential Changes during Brain Retraction in Dogs. *Stroke* **1977**, *8*, 487–492. [[CrossRef](#)]
3. Andrews, R.J.; Bringas, J.R. A Review of Brain Retraction and Recommendations for Minimizing Intraoperative Brain Injury. *Neurosurgery* **1993**, *33*, 1052–1064. [[CrossRef](#)]
4. Spetzler, R.F.; Sanai, N. The Quiet Revolution: Retractorless Surgery for Complex Vascular and Skull Base Lesions: Clinical Article. *J. Neurosurg.* **2012**, *116*, 291–300. [[CrossRef](#)]
5. Rice, B.J.; Peerless, S.J.; Drake, C.G. Surgical Treatment of Unruptured Aneurysms of the Posterior Circulation. *J. Neurosurg.* **1990**, *73*, 165–173. [[CrossRef](#)]
6. Nazzaro, J.M.; Shults, W.T.; Neuwelt, E.A. Neuro-Ophthalmological Function of Patients with Pineal Region Tumors Approached Transtentorially in the Semisitting Position. *J. Neurosurg.* **1992**, *76*, 746–751. [[CrossRef](#)]
7. Laha, R.K.; Dujovny, M.; Rao, S.; Barrionuevo, P.J.; Bunegin, L.; Hellstrom, H.R.; Albin, M.S.; Taylor, F.H. Cerebellar Retraction: Significance and Sequelae. *Surg. Neurol.* **1979**, *12*, 209–215.
8. Bell, B.A.; Symon, L.; Branston, N.M. CBF and Time Thresholds for the Formation of Ischemic Cerebral Edema, and Effect of Reperfusion in Baboons. *J. Neurosurg.* **1985**, *62*, 31–41. [[CrossRef](#)]
9. Fukamachi, A.; Koizumi, H.; Nukui, H. Postoperative Intracerebral Hemorrhages: A Survey of Computed Tomographic Findings after 1074 Intracranial Operations. *Surg. Neurol.* **1985**, *23*, 575–580. [[CrossRef](#)]
10. Hu, X.; Chen, A.; Luo, Y.; Zhang, C. Steerable catheters for minimally invasive surgery: A review and future directions. *Comput. Assist. Surg.* **2018**, *23*, 21–41. [[CrossRef](#)]
11. Kalfas, I.H.; Little, J.R. Postoperative Hemorrhage: A Survey of 4992 Intracranial Procedures. *Neurosurgery* **1988**, *23*, 343–347. [[CrossRef](#)]
12. Rosenørn, J. The Risk of Ischaemic Brain Damage during the Use of Self-Retaining Brain Retractors. *Acta Neurol. Scand.* **1989**, *79*, 1–30. [[CrossRef](#)]
13. Dai, Z. Improvement of General Design Theory and Methodology with Its Application to Design of a Retractor for Ventral Hernia Repair Surgery. Master's Thesis, University of Saskatchewan, Saskatoon, SK, Canada, March 2019.
14. Yokoh, A.; Sugita, K.; Kobayashi, S. Clinical Study of Brain Retraction in Different Approaches and Diseases. *Acta Neurochir.* **1987**, *87*, 134–139. [[CrossRef](#)]
15. Dujovny, M.; Wackenhut, N.; Kossovsky, N.; Leff, L.; Gómez, C.; Nelson, D. Biomechanics of Vascular Occlusion in Neurosurgery. *Acta Neurol. Lat.* **1980**, *26*, 123–127.
16. DeLorenzo, C.; Papademetris, X.; Staib, L.H.; Vives, K.P.; Spencer, D.D.; Duncan, J.S. Volumetric Intraoperative Brain Deformation Compensation: Model Development and Phantom Validation. *IEEE Trans. Med. Imaging* **2012**, *31*, 1607–1619. [[CrossRef](#)]
17. Hartkens, T.; Hill, D.L.G.; Castellano-Smith, A.D.; Hawkes, D.J.; Maurer, C.R.; Martin, A.J.; Hall, W.A.; Liu, H.; Truwit, C.L. Measurement and Analysis of Brain Deformation during Neurosurgery. *IEEE Trans. Med. Imaging* **2003**, *22*, 82–92. [[CrossRef](#)]
18. Warfield, S.K.; Talos, F.; Tei, A.; Bharatha, A.; Nabavi, A.; Ferrant, M.; McL. Black, P.; Jolesz, F.A.; Kikinis, R. Real-Time Registration of Volumetric Brain MRI by Biomechanical Simulation of Deformation during Image Guided Neurosurgery. *Comput. Vis. Sci.* **2002**, *5*, 3–11. [[CrossRef](#)]
19. Arani, A.; Min, H.-K.; Fattahi, N.; Wetjen, N.M.; Trzasko, J.D.; Manduca, A.; Jack, C.R.; Lee, K.H.; Ehman, R.L.; Huston, J. Acute Pressure Changes in the Brain Are Correlated with MR Elastography Stiffness Measurements: Initial Feasibility in an in Vivo Large Animal Model: MRE Stiffness Correlates With Changes in ICP. *Magn. Reson. Med.* **2018**, *79*, 1043–1051. [[CrossRef](#)]
20. Budday, S.; Ovaert, T.C.; Holzapfel, G.A.; Steinmann, P.; Kuhl, E. Fifty Shades of Brain: A Review on the Mechanical Testing and Modeling of Brain Tissue. *Arch. Comput. Methods Eng.* **2020**, *27*, 1187–1230. [[CrossRef](#)]
21. Chambers, I.R.; Martin, D.; Clark, A.; Nicklin, A.; Mendelow, A.D.; Mitchell, P. The Measurement of Brain Tissue Stiffness In-Vivo. In *Acta Neurochirurgica Supplements*; Steiger, H.-J., Ed.; Acta Neurochirurgica Supplementum; Springer: Vienna, Austria, 2008; Volume 102, pp. 287–289. ISBN 978-3-211-85577-5.
22. Fallah, A.; Subramaniam, T.; Phillips, H.W.; Michalet, X.; Vinters, H.V.; Yong, W.H.; Wu, J.Y.; Salamon, N.; Ellingson, B.M.; Wang, A.C.; et al. Novel Tonometer Device Distinguishes Brain Stiffness in Epilepsy Surgery. *Sci. Rep.* **2020**, *10*, 20978. [[CrossRef](#)]
23. Kyriacou, S.K.; Mohamed, A.; Miller, K.; Neff, S. Brain Mechanics For Neurosurgery: Modeling Issues. *Biomech. Model. Mechanobiol.* **2002**, *1*, 151–164. [[CrossRef](#)] [[PubMed](#)]
24. Cepolina, F.; Razzoli, R.P. An introductory review of robotically assisted surgical systems. *Int. J. Med. Robot.* **2022**, *18*, e2409. [[CrossRef](#)] [[PubMed](#)]
25. Hoeckelmann, M.; Rudas, I.J.; Fiorini, P.; Kirchner, F.; Haidegger, T. Current Capabilities and Development Potential in Surgical Robotics. *Int. J. Adv. Robot. Syst.* **2015**, *12*, 61. [[CrossRef](#)]
26. Attanasio, A.; Scaglioni, B.; De Momi, E.; Fiorini, P.; Valdastris, P. Autonomy in Surgical Robotics. *Annu. Rev. Control Robot. Auton. Syst.* **2021**, *4*, 651–679. [[CrossRef](#)]

27. Davies, B.; Starkie, S.; Harris, S.J.; Agterhuis, E.; Paul, V.; Auer, L.M. Neurobot: A Special-Purpose Robot for Neurosurgery. In Proceedings of the 2000 ICRA. Millennium Conference. IEEE International Conference on Robotics and Automation. Symposia Proceedings (Cat. No.00CH37065), San Francisco, CA, USA, 24–28 April 2000; Volume 4, pp. 4103–4108.
28. Švaco, M.; Koren, P.; Jerbić, B.; Vidaković, J.; Šekoranja, B.; Šuligoj, F. Validation of Three KUKA Agilus Robots for Application in Neurosurgery. In *Advances in Service and Industrial Robotics*; Ferraresi, C., Quaglia, G., Eds.; Mechanisms and Machine Science; Springer International Publishing: Cham, Switzerland, 2018; Volume 49, pp. 996–1006. ISBN 978-3-319-61275-1.
29. Okamoto, J.; Iida, M.; Nambu, K.; Fujie, M.G.; Umezū, M. Development of Multi-Dof Brain Retractor Manipulator with Safety Method. In Proceedings of the 2003 IEEE/RSJ International Conference on Intelligent Robots and Systems (IROS 2003) (Cat. No.03CH37453), Las Vegas, NV, USA, 27–31 October 2003; Volume 3, pp. 2594–2599.
30. Watanabe, M.; Yoneyama, T.; Nakada, M.; Watanabe, T. Development of Disposable Pressure Sensible Retractor System for Preventing the Overloading. In Proceedings of the 2019 IEEE/SICE International Symposium on System Integration (SII), Paris, France, 14–16 January 2019; pp. 129–134.
31. Malone, H.R.; Syed, O.N.; Downes, M.S.; D’Ambrosio, A.L.; Quest, D.O.; Kaiser, M.G. Simulation in Neurosurgery: A Review of Computer-Based Simulation Environments and Their Surgical Applications. *Neurosurgery* **2010**, *67*, 1105–1116. [[CrossRef](#)] [[PubMed](#)]
32. Sase, K.; Fukuhara, A.; Tsujita, T.; Konno, A. GPU-Accelerated Surgery Simulation for Opening a Brain Fissure. *Robomech J.* **2015**, *2*, 17. [[CrossRef](#)]
33. Coats, B.; Margulies, S.S. Material Properties of Porcine Parietal Cortex. *J. Biomech.* **2006**, *39*, 2521–2525. [[CrossRef](#)]
34. Ying, H.S.; Liu, P.X.; Hou, W.G. A deformation model of pulsating brain tissue for neurosurgery simulation. *Comput. Methods Programs Biomed.* **2022**, *218*, 106729. [[CrossRef](#)]
35. Gan, L.S.; Zareinia, K.; Lama, S.; Maddahi, Y.; Yang, F.W.; Sutherland, G.R. Quantification of Forces During a Neurosurgical Procedure: A Pilot Study. *World Neurosurg.* **2015**, *84*, 537–548. [[CrossRef](#)]
36. Miller, K.; Wittek, A.; Joldes, G.; Horton, A.; Dutta-Roy, T.; Berger, J.; Morriss, L. Modelling Brain Deformations for Computer-Integrated Neurosurgery. *Int. J. Numer. Meth. Biomed. Eng.* **2010**, *26*, 117–138. [[CrossRef](#)]

**Disclaimer/Publisher’s Note:** The statements, opinions and data contained in all publications are solely those of the individual author(s) and contributor(s) and not of MDPI and/or the editor(s). MDPI and/or the editor(s) disclaim responsibility for any injury to people or property resulting from any ideas, methods, instructions or products referred to in the content.